

Journal of Materials Chemistry C

Accepted Manuscript



This is an *Accepted Manuscript*, which has been through the Royal Society of Chemistry peer review process and has been accepted for publication.

Accepted Manuscripts are published online shortly after acceptance, before technical editing, formatting and proof reading. Using this free service, authors can make their results available to the community, in citable form, before we publish the edited article. We will replace this *Accepted Manuscript* with the edited and formatted *Advance Article* as soon as it is available.

You can find more information about *Accepted Manuscripts* in the [Information for Authors](#).

Please note that technical editing may introduce minor changes to the text and/or graphics, which may alter content. The journal's standard [Terms & Conditions](#) and the [Ethical guidelines](#) still apply. In no event shall the Royal Society of Chemistry be held responsible for any errors or omissions in this *Accepted Manuscript* or any consequences arising from the use of any information it contains.



www.rsc.org/materialsC

ARTICLE

Mechanofluorochromic properties of β -iminoenolate boron complexes tuned by the electronic effects of terminal phenothiazine and phenothiazine-*S,S*-dioxide

Cite this: DOI: 10.1039/x0xx00000x

Received 00th January 2012,

Accepted 00th January 2012

DOI: 10.1039/x0xx00000x

www.rsc.org/Zhenqi Zhang,^a Zhu Wu,^a Jingbo Sun,^a Boqi Yao,^a Gonghe Zhang,^a Pengchong Xue^a and Ran Lu^{a*}

β -Iminoenolate boron complexes bearing non-planar phenothiazine (**P2B** and **P16B**) and phenothiazine-*S,S*-dioxide (**PO2B** and **PO16B**) have been synthesized. It was found that **P2B** and **P16B** gave ICT emission due to the strong electron-donating ability of phenothiazine, and no ICT emission was detected for **PO2B** and **PO16B** because of weak electron-donating ability of phenothiazine-*S,S*-dioxide. In particular, **P2B** and **P16B** exhibited high-contrast MFC behaviors compared with that of **PO2B**. On account of the formation of π -aggregates in the as-synthesized crystals of **P2B**, several channels for the changes of emitting colors in different solid states were provided. The as-synthesized crystals of **P2B** emitting weak brown light could be changed into ground powders emitting deep orange-red light after grinding. When the ground powders were fumed with DCM for 5 s or heated at 160 °C for 3 s, the samples emitted yellow and yellowish green light, respectively. Although the π -conjugated skeleton of **P16B** was same as that of **P2B**, the introduction of long carbon chain led to different MFC properties. The as-synthesized crystals of **P16B** emitting yellow light could be changed into ground powders emitting orange light upon grinding. Particularly, the amorphous state of **P16B** could be self-recovered to crystalline state when put at room temperature for 5 min because the π - π interactions might be restrained by long carbon chain, leading to low stability of amorphous state. In the case of **PO2B**, low-contrast and reversible MFC properties were observed under grinding/fuming or heating treatment. No mechanofluorochromism was observed for **PO16B** since long carbon chain was involved and no ICT emission happened. Therefore, we suggested that the introduction of non-planar conjugated unit and the construction of D- π -A system with ICT emission were favorable for designing MFC dyes with high-contrast changes in emitting colors in different solid states, and the introduction of long carbon chain could improve the MFC reversibility so as to gain self-recovering MFC materials.

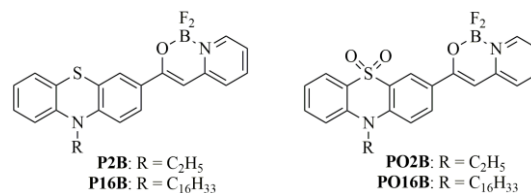
Introduction

Mechanofluorochromic (MFC) materials, whose emitting colors could be changed under external mechanical stimuli, such as stretching, grinding, pressing and shearing,¹ have gained increasing interests due to their potential applications in luminescence switches,² mechanosensors³ and optoelectronic devices.⁴ It was found that the changes of the solid emission were induced by the transformation of the molecular packing mode or molecular conformation instead of chemical structure change, so the mechanofluorochromism was usually reversible. Tian *et al* investigated the relationship between the solid emission behaviors of 9,10-bis(*E*)-2-(pyrid-2-yl)vinyl)anthracene and the external pressure, and suggested

that the emission could be tuned by the crystal states.⁵ Tang and coworkers synthesized triphenylacrylonitrile derivatives and found that the twisted propeller-like conformations and the intermolecular interactions not only endowed the luminogens with AIE characteristics, but also rendered them to undergo conformational planarization upon mechanical stimuli, resulting in remarkable changes in emitting color and fluorescence efficiency.^{6a} Moreover, other kinds of MFC dyes, including tetraphenylethene derivatives,⁶ 9,10-divinylanthracene derivatives,⁷ oligo(*p*-phenylene vinylene) derivatives⁸ and β -diketone boron complexes⁹ have been reported. It was known that non-planar π -conjugated structure played a key role in realizing mechanofluorochromism because of their loose molecular packing in crystals which can be damaged easily

under external stimuli.^{6,10,11} In our previous work, we reported the MFC properties of benzoxazole derivatives bearing non-planar triphenylamine or phenothiazine,^{10a,11a} as well as the triphenylacrylonitrile derivatives functionalized with phenothiazine.^{11d} We found that the D- π -A system with ICT emission might exhibit MFC behaviors. Herein, phenothiazine was selected as a building block in target molecules because it was a strong electron donor with a non-planar butterfly conformation and had wide potential applications in dye-sensitized solar cells,¹² chemosensors,¹³ near-infrared emitting materials¹⁴ and self-assembling systems.¹⁵ On the other hand, although the oxidized phenothiazine, such as phenothiazine-*S,S*-dioxide, has been introduced in polymers to be used as near-infrared emitting materials and emitting layers in OLED,¹⁶ to the best of our knowledge, the MFC dye bearing phenothiazine-*S,S*-dioxide has not been reported. Considering the same conformation of phenothiazine-*S,S*-dioxide and phenothiazine, it provided us a platform to discuss the exclusive effect of electronic structures on MFC properties of the dyes. Additionally, the organic boron complexes, including N,N-O,O- and N,O-chelated boron complexes, were excellent fluorophores. Among them, the N,N-chelated boron complexes of BODIPY derivatives were widely used in sensors,¹⁷ solar cells¹⁸ and near-infrared materials,¹⁹ and the O,O-chelated boron complexes have been found to exhibit better self-assembling, MFC and fluorescence sensory properties.²⁰ It should be noted that the N,O-chelated boron complexes have attracted recent attention on account of the diversity of the ligands, variety of the structures and intense emission in solutions and solid states.²¹ We have found that carbazole functionalized β -iminoenolate boron complexes with ICT emission showed obvious MFC properties.^{11b} With these in mind, we designed new β -iminoenolate boron complexes functionalized with phenothiazine (**P2B** and **P16B**) and phenothiazine-*S,S*-dioxide (**PO2B** and **PO16B**, Scheme 1). Thus, we could reveal how the electronic effect of phenothiazine and phenothiazine-*S,S*-dioxide affected MFC behaviors of the dyes regardless of the effect of the conformation of π -skeleton. On the other hand, the length of alky chain often played a key role in the molecular packing mode to lead to various emission in different solid states,^{11c,22} so ethyl and hexadecyl were introduced in 10-position of phenothiazine and phenothiazine-*S,S*-dioxide. It was found that **P2B** with ICT emission exhibited high-contrast MFC behaviors. For example, the as-synthesized crystals of **P2B** emitting weak brown light could be changed into ground powders emitting deep orange-red light after grinding. When the ground powders were fumed by DCM for 5 s or heated at 160 °C for 3 s, the samples emitted yellow and yellowish green light, respectively. However, **PO2B** without ICT emission gave low-contrast MFC properties, for instance, the as-synthesized crystals emitting yellow light could be transformed into amorphous state emitting yellowish green light after grinding. In the case of **P16B** with same conjugated skeleton as **P2B**, the as-synthesized crystals emitted bright yellow light, and the emitting color changed into orange after grinding, indicating

that high-contrast changes of the emitting colors would be fulfilled in different solid states of the dye with ICT emission. Moreover, the ground powders of **P16B** could be self-recovered into crystalline state when put at room temperature for 5 min. It suggested that long carbon chain would decrease the stability of amorphous state. As a result, no MFC property was detected for **PO16B**, in which long carbon chain was involved, without ICT emission.



Scheme 1. Molecular structures of β -iminoenolate boron complexes.

Experimental Section

Measurement and characterization. ¹H NMR spectra were measured with a Mercury Plus instrument at 400 MHz by using DMSO-*d*₆ as solvent in all cases. ¹³C NMR spectra were measured with a Mercury Plus instrument at 100 MHz and 125 M by using CDCl₃ and DMSO-*d*₆ as solvents. FT-IR spectra were measured with a Nicolet-360 FT-IR spectrometer by incorporation of samples in KBr disks. The UV-vis absorption spectra were obtained on Shimadzu UV-3100 spectrophotometer. Fluorescent emission spectra were obtained on a Cary Eclipse fluorescence spectrophotometer. Mass spectra were obtained with Agilent 1100 MS series and AXIMA CFR MALDI-TOF (Compact) mass spectrometers. C, H, and N elemental analyses were performed with a Perkin-Elmer 240C elemental analyzer. XRD patterns were obtained on an Empyrean X-ray diffraction instrument. Cyclic voltammograms were obtained on a CHI 604C voltammetric analyzer with a scan rate at 50 mV/s. A three electrode configuration was used for the measurement: a platinum button as the working electrode, a platinum wire as the counter electrode, and a saturated calomel electrode (SCE) as the reference electrode. The solution of (C₄H₉)₄NBF₄ in CH₂Cl₂ (0.1 M) was used as the supporting electrolyte.

Materials: THF was dried over sodium and diphenyl ketone. DCM was dried over calcium hydride. The other chemicals and reagents were used as received without further purification. Compounds **1a**, **1b**, **3a** and **3b** were synthesized according to the literatures.^{14b,15,23}

Ethyl 10-ethyl-10H-phenothiazine-3-carboxylate (2a): Concentrated sulfuric acid (1 mL) was added dropwise to the solution of **1a** (1.00 g, 4.00 mmol) in ethanol (30 mL) with stirring. The mixture was refluxed for 5 h, and was then poured into water (200 mL) and extracted with DCM. After removal of the solvent, the crude product was purified by column chromatography (silica gel, petroleum ether/ethyl acetate, v/v = 3/1) to afford **2a** (0.91 g) as a dark green liquid. Yield 75%; ¹H

NMR (400 MHz, DMSO- d_6) δ 7.76 (dd, J = 8.6 Hz, 2.0 Hz, 1H), 7.60 (d, J = 2.0 Hz, 1H), 7.22 (m, 1H), 7.14 (dd, J = 7.6 Hz, 1.5 Hz, 1H), 7.07 (t, J = 8.6 Hz, 2H), 6.98 (t, J = 7.5 Hz, 1H), 4.26 (q, J = 7.1 Hz, 2H), 3.96 (q, J = 6.9 Hz, 2H), 1.30 (td, J = 7.0 Hz, 3.9 Hz, 6H) (Figure S16); MALDI-TOF MS: m/z : calculated for $C_{17}H_{17}NO_2S$: 299.1; found: 300.3 ($[M+H]^+$) (Figure S17).

Ethyl 10-hexadecyl-10H-phenothiazine-3-carboxylate (2b):

Following the synthetic procedure of **2a**, compound **2b** (0.88 g) was prepared through alcoholysis of **1b** (1.00 g, 2.23 mmol) with ethanol (30 mL) catalyzed by concentrated sulfuric acid (1 mL). Crude product was purified by column chromatography (silica gel, petroleum ether/ethyl acetate, v/v = 6/1) to afford a dark yellow green liquid. Yield 80%; 1H NMR (400 MHz, DMSO- d_6) δ 7.76 (d, J = 8.6 Hz, 1H), 7.62 (s, 1H), 7.22 (t, J = 7.6 Hz, 1H), 7.15 (d, J = 7.4 Hz, 1H), 7.07 (t, J = 9.7 Hz, 2H), 6.98 (t, J = 7.4 Hz, 1H), 4.26 (q, J = 7.0 Hz, 2H), 3.91 (t, J = 6.7 Hz, 2H), 1.67 (m, 2H), 1.28 (m, 29H), 0.85 (t, J = 6.4 Hz, 3H) (Figure S18); MALDI-TOF MS: m/z : calculated for $C_{31}H_{45}NO_2S$: 495.3; found: 496.9 ($[M+H]^+$) (Figure S19).

3-(10-ethyl-10H-phenothiazin-3-yl)-1,1-difluoro-1H-pyrido[1,2-c][1,3,2]oxazaborinin-9-ium-1-uide (P2B):

NaH (60 %, 0.21 g, 5.34 mmol) was added to a solution of 2-methyl pyridine (0.64 mL, 5.34 mmol) in THF (50 mL) at 0 °C, and compound **2a** (0.80 g, 2.67 mmol) was then added. The mixture was stirred at room temperature for 30 min. After the mixture was refluxed under an atmosphere of nitrogen for another 24 h, it was cooled to room temperature. The mixture was poured into water and acidified with dilute HCl. The obtained yellow solid was collected by suction filtration, and dried under vacuum. After the solid was dissolved in DCM (50 mL), boron trifluoride diethyl ether complex (1.00 mL, 8.01 mmol) and triethylamine (1.12 mL, 8.01 mmol) were added under an atmosphere of nitrogen. After the mixture was stirred at room temperature for 24 h, water (200 mL) was added in order to quench the reaction. The organic layer was separated and dried over anhydrous Na_2SO_4 . After removal of the solvent, the crude product was purified by column chromatography (silica gel, DCM/petroleum ether, v/v = 3/1) to afford **P2B** (0.44 g) as a brown solid. Yield: 42%; m.p. 197.0-199.0 °C; 1H NMR (400 MHz, DMSO- d_6) δ 8.46 (d, J = 5.9 Hz, 1H), 8.18 (m, 1H), 7.75 (dd, J = 8.6 Hz, 2.1 Hz, 1H), 7.65 (d, J = 2.1 Hz, 1H), 7.59 (d, J = 8.3 Hz, 1H), 7.51 (t, J = 6.7 Hz, 1H), 7.22 (m, 1H), 7.16 (dd, J = 7.16 Hz, 1.3 Hz, 1H), 7.11 (d, J = 8.7 Hz, 1H), 7.06 (d, J = 8.0 Hz, 1H), 6.97 (t, J = 7.4 Hz, 1H), 6.83 (s, 1H), 3.97 (q, J = 6.9 Hz, 2H), 1.33 (t, J = 6.9 Hz, 3H) (Figure S20); ^{13}C NMR (100 MHz, $CDCl_3$) δ 161.92, 151.76, 147.20, 143.78, 141.03, 139.67, 127.97, 127.45, 127.40, 126.17, 125.21, 123.93, 123.47, 122.94, 122.28, 119.63, 115.28, 114.48, 91.90, 42.31, 12.86 (Figure S21); MALDI-TOF MS: m/z : calculated for $C_{21}H_{17}BF_2N_2OS$: 394.1; found: 395.0 ($[M+H]^+$) (Figure S22) elemental analysis (%) calculated for $C_{21}H_{17}BF_2N_2OS$: C 63.98, H 4.35, N 7.11; found: C 64.05, H 4.42, N 7.14; FT-IR (KBr, cm^{-1}): 756, 763, 916, 1033, 1128, 1209, 1233, 1253, 1283, 1332,

1378, 1408, 1444, 1464, 1493, 1541, 1575, 1610, 1628, 2868, 2933, 2982, 3054.

3-(10-hexadecyl-10H-phenothiazin-3-yl)-1,1-difluoro-1H-pyrido[1,2-c][1,3,2]oxazaborinin-9-ium-1-uide (P16B):

Following the synthetic procedure of **P2B**, the intermediate was synthesized from **2b** (1.00 g, 2.02 mmol) and 2-methyl pyridine (0.48 mL, 4.04 mmol) in THF. Then the intermediate was reacted with boron trifluoride diethyl ether complex (0.76 mL, 6.06 mmol) in the presence of triethylamine (0.85 mL, 6.06 mmol) in DCM. The crude product was purified by column chromatography (silica gel, DCM/petroleum ether, v/v = 1/1) to afford **P16B** (0.45 g) as a yellow solid. Yield 38%; m.p. 73.0-74.0 °C; 1H NMR (400 MHz, DMSO- d_6) δ 8.47 (d, J = 5.9 Hz, 1H), 8.18 (t, J = 7.8 Hz, 1H), 7.76 (dd, J = 8.6 Hz, 2.0 Hz, 1H), 7.66 (d, J = 2.1 Hz, 1H), 7.59 (d, J = 8.3 Hz, 1H), 7.51 (t, J = 7.1 Hz, 1H), 7.22 (t, J = 7.7 Hz, 1H), 7.16 (d, J = 7.6 Hz, 1H), 7.10 (d, J = 8.7 Hz, 1H), 7.05 (d, J = 8.2 Hz, 1H), 6.98 (t, J = 7.5 Hz, 1H), 6.83 (s, 1H), 3.92 (t, J = 6.6 Hz, 2H), 1.69 (m, 2H), 1.38 (m, 2H), 1.20 (m, 24H), 0.84 (t, J = 6.8 Hz, 3H) (Figure S23); ^{13}C NMR (125 MHz, $CDCl_3$) δ 162.19, 151.86, 147.68, 144.21, 140.94, 139.76, 127.47, 127.36, 126.14, 125.31, 122.92, 122.20, 119.53, 115.59, 114.83, 91.81, 47.72, 31.94, 29.70, 29.63, 29.53, 29.36, 29.22, 26.88, 26.78, 22.69, 14.11 (Figure S24); MALDI-TOF MS: m/z : calculated for $C_{37}H_{45}BF_2N_2OS$: 590.33; found: 591.6 ($[M+H]^+$) (Figure S25); elemental analysis (%) calculated for $C_{37}H_{45}BF_2N_2OS$: C 71.18, H 7.68, N 4.74; found: C 73.24, H 8.05, N 4.78; FT-IR (KBr, cm^{-1}): 762, 802, 920, 1034, 1083, 1123, 1175, 1212, 1334, 1383, 1445, 1464, 1497, 1543, 1576, 1603, 1627, 2849, 2921.

10-ethyl-10H-phenothiazine-3-carboxylic acid 5,5-dioxide (4a):

Compound **3a** (1.50 g, 5.87 mmol) was dissolved in the mixed solvent of THF (10 mL) and water (10 mL). Potassium permanganate was added to the solution in portion at 60 °C. It was found that the purple color for the potassium permanganate solution changed into brown quickly when it was added to the mixture. The reaction was completed until the purple color could not be changed. Then, the mixture was filtrated and the residue was washed with THF and water several times. After that, the filtrate was concentrated and poured into water. After acidified with dilute HCl, white precipitate was collected by filtration. The crude product (1.46 g) as a white solid was obtained without further purification due to its poor solubility. Yield ca. 82 %; MALDI-TOF MS: m/z : calculated for $C_{15}H_{13}NO_4S$: 303.1; found: 301.8 ($[M-H]^+$) (Figure S26).

10-hexadecyl-10H-phenothiazine-3-carboxylic acid 5,5-dioxide (4b):

Following the synthetic procedure of **4a**, compound **4b** was synthesized from **3b** (1.20 g, 2.66 mmol) via oxidation reaction. The crude product (1.04 g) as a white solid was obtained without further purification due to its poor solubility. Yield 78%; MALDI-TOF MS: m/z : calculated for $C_{29}H_{41}NO_4S$: 499.3; found: 498.3 ($[M-H]^+$) (Figure S27).

Methyl 10-ethyl-10H-phenothiazine-3-carboxylate 5,5-dioxide (5a): Concentrated sulfuric acid (1 mL) was added dropwise in the solution of **4a** (1.00 g, 3.30 mmol) in methanol (30 mL) with stirring. After refluxed for 5 h, the mixture was poured into water (200 mL). The precipitate was obtained by filtration, followed by recrystallization in ethanol to afford **5a** as a white solid (0.82 g). Yield 78%; ¹H NMR (400 MHz, DMSO-*d*₆) δ 8.49 (d, *J* = 2.1 Hz, 1H), 8.25 (dd, *J* = 9.1 Hz, 2.1 Hz, 1H), 8.07 (dd, *J* = 7.9 Hz, 1.5 Hz, 1H), 7.82 (m, 3H), 7.45 (t, *J* = 7.4 Hz, 1H), 4.43 (q, *J* = 7.0 Hz, 2H), 3.91 (s, 3H), 1.44 (t, *J* = 7.0 Hz, 3H) (Figure S28); MALDI-TOF MS: *m/z*: calculated for C₁₆H₁₅NO₄S: 317.1; found: 316.2 ([M-H]⁺) (Figure S29)

Ethyl 10-hexadecyl-10H-phenothiazine-3-carboxylate 5,5-dioxide (5b): Following the synthetic procedure of **5a**, compound **5b** was synthesized from **4b** (1.00 g, 2.2 mmol) and ethanol. When the reaction was complete, the mixture was poured into water (200 mL) and extracted by DCM. After removal of the solvent, the crude product was purified by column chromatography (silica gel, petroleum ether/ethyl acetate, *v/v* = 3/1) to afford a pale yellow liquid (0.82 g). Yield 72%; ¹H NMR (400 MHz, DMSO-*d*₆) δ 8.47 (d, *J* = 1.9 Hz, 1H), 8.23 (dd, *J* = 9.0 Hz, 1.9 Hz, 1H), 8.04 (d, *J* = 7.9 Hz, 1H), 7.78 (m, 3H), 7.44 (t, *J* = 7.4 Hz, 1H), 4.36 (q, *J* = 7.0 Hz, 4H), 1.75 (dd, *J* = 14.3 Hz, 7.4 Hz, 2H), 1.29 (m, 29H), 0.84 (t, *J* = 6.7 Hz, 3H) (Figure S30); MALDI-TOF MS: *m/z*: calculated for C₃₁H₄₅NO₄S: 527.3; found: 526.7 ([M-H]⁺) (Figure S31).

3-(10-ethyl-5,5-dioxido-10H-phenothiazin-3-yl)-1,1-difluoro-1H-pyrido[1,2-*c*][1,3,2]oxazaborinin-9-ium-1-uide (PO2B): Following the synthetic procedure of **P2B**, the intermediate was synthesized from **5a** (1.00 g, 3.15 mmol) and 2-methyl pyridine (0.75 mL, 6.30 mmol) in THF. Then the intermediate was reacted with boron trifluoride diethyl ether complex (1.19 mL, 9.45 mmol) in the presence of triethylamine (1.33 mL, 9.45 mmol) in DCM. The crude product was purified by column chromatography (silica gel, DCM/ethyl acetate, *v/v* = 5/1) to afford **PO2B** (0.54 g) as a yellow solid. Yield 40%; m.p. 276.0–278.0 °C; ¹H NMR (400 MHz, DMSO-*d*₆) δ 8.54 (d, *J* = 5.8 Hz, 1H), 8.47 (d, *J* = 2.1 Hz, 1H), 8.26 (m, 2H), 8.07 (dd, *J* = 7.9 Hz, 1.3 Hz, 1H), 7.80 (m, 2H), 7.73 (dd, *J* = 14.5 Hz, 8.4 Hz, 2H), 7.58 (t, *J* = 6.4 Hz, 1H), 7.42 (t, *J* = 6.4 Hz, 1H), 7.08 (s, 1H), 4.43 (q, *J* = 6.9 Hz, 2H), 1.44 (t, *J* = 6.9 Hz, 3H) (Figure S32); ¹³C NMR (125 MHz, DMSO-*d*₆) δ 158.30, 150.92, 143.50, 141.54, 140.40, 139.79, 134.52, 131.19, 127.42, 123.72, 123.61, 123.42, 123.35, 123.10, 122.45, 120.75, 117.84, 117.54, 94.14, 43.19, 12.58 (Figure S33); MALDI-TOF MS: *m/z*: calculated for C₂₁H₁₇BF₂N₂O₃S: 426.1; found: 427.2 ([M+H]⁺) (Figure S34); elemental analysis (%) calculated for C₂₁H₁₇BF₂N₂O₃S: C 59.17, H 4.02, N 6.57; found: C 59.22, H 4.09, N 6.59; FT-IR (KBr, cm⁻¹): 756, 798, 925, 1034, 1090, 1128, 1143, 1165, 1216, 1286, 1348, 1388, 1419, 1470, 1497, 1546, 1594, 1615, 1633, 2928, 2981, 3057, 3085.

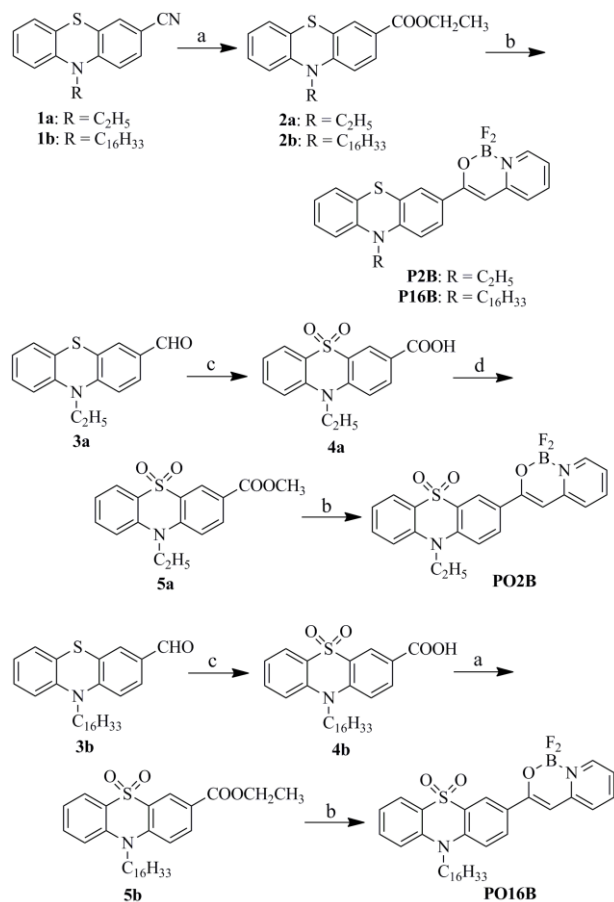
3-(10-hexadecyl-5,5-dioxido-10H-phenothiazin-3-yl)-1,1-difluoro-1H-pyrido[1,2-*c*][1,3,2]oxazaborinin-9-ium-1-uide

(PO16B): Following the synthetic procedure of **P2B**, the intermediate was synthesized from **5b** (1.00 g, 1.61 mmol) and 2-methyl pyridine (0.38 mL, 3.22 mmol) in THF. Then, the intermediate was reacted with boron trifluoride diethyl ether complex (0.61 mL, 4.83 mmol) in the presence of triethylamine (0.68 mL, 4.83 mmol) in DCM. The crude product was purified by column chromatography (silica gel, DCM/ethyl acetate, *v/v* = 20/1) to afford **PO16B** (0.43 g) as a yellow solid. Yield 43%; m.p. 168.0–170.0 °C; ¹H NMR (400 MHz, DMSO-*d*₆) δ 8.55 (d, *J* = 5.9 Hz, 1H), 8.48 (d, *J* = 2.1 Hz, 1H), 8.24 (m, 2H), 8.06 (dd, *J* = 7.8 Hz, 1.3 Hz, 1H), 7.79 (m, 2H), 7.71 (d, *J* = 8.9 Hz, 2H), 7.58 (t, *J* = 6.7 Hz, 1H), 7.41 (t, *J* = 7.5 Hz, 1H), 7.07 (s, 1H), 4.35 (t, *J* = 7.2 Hz, 2H), 1.76 (m, 2H), 1.37 (m, 2H), 1.17 (m, 24H), 0.82 (t, *J* = 6.8 Hz, 3H) (Figure S35); ¹³C NMR (100 MHz, CDCl₃) δ 160.34, 151.40, 141.99, 141.51, 140.30, 139.93, 133.42, 131.12, 127.62, 124.31, 123.93, 123.75, 122.63, 122.40, 121.94, 120.44, 116.24, 116.19, 93.04, 48.66, 31.95, 29.72, 29.69, 29.65, 29.57, 29.39, 29.23, 22.72, 14.16 (Figure S36); MALDI-TOF MS: *m/z*: calculated for C₃₅H₄₅BF₂N₂O₃S: 622.3; found: 623.6 ([M+H]⁺) (Figure S37); elemental analysis (%) calculated for C₃₅H₄₅BF₂N₂O₃S: C 67.52, H 7.28, N 4.50; found: C 67.96, H 7.54, N 4.53; FT-IR (KBr, cm⁻¹): 561, 577, 634, 659, 716, 773, 816, 918, 1030, 1089, 1133, 1147, 1177, 1220, 1288, 1370, 1393, 1421, 1471, 1498, 1549, 1594, 1614, 1631, 2852, 2916.

Results and Discussion

Synthesis: The synthetic routes of β-iminoenolate boron complexes **P2B**, **P16B**, **PO2B** and **PO16B** were shown in Scheme 1. Compounds **1a**, **1b**, **3a** and **3b** were synthesized according to the literatures.^{14b,15,23} **2a** and **2b** were synthesized via the alcoholysis reactions of **1a** and **1b** catalyzed by concentrated sulfuric acid in yields of 75% and 80%, respectively. The condensation reaction between ester **2a** and 2-methyl pyridine catalyzed by NaH afforded an intermediate, which was not further purified and complexed with boron trifluoride diethyl ether directly in the presence of triethylamine to afford **P2B** in a yield of 42%. Similarly, **P16B** was prepared from **2b**, 2-methyl pyridine and boron trifluoride diethyl ether in a yield of 38%. **4a** and **4b** were synthesized via the oxidation reactions of **3a** and **3b** with potassium permanganate, respectively, in yields of 82% and 78%. The crude products of carboxylic acids **4a** and **4b** were easily adhered to the powers of MnO₂, so the filter cake should be washed with THF for several times. **5a** and **5b** were obtained by the esterification of **4a** and **4b** catalyzed by concentrated sulfuric acid. According to the synthetic procedures of **P2B**, **PO2B** and **PO16B** were gained from the condensation reaction between ester **5a/5b** and 2-methyl pyridine, followed by complexation with boron trifluoride diethyl ether. The target molecules were characterized by ¹H-NMR, ¹³C-NMR, MALDI-TOF, elemental analysis and FT-IR. **P2B**, **PO2B** and **PO16B** could be well dissolved in the solvents of toluene, DCM and DMSO. **PO2B**

showed limited solubility in chloroform (1.0 mg/mL) and DMSO (2.0 mg/mL).



(a) CH₃CH₂OH, H₂SO₄, reflux; (b) i) 2-methyl pyridine, NaH, THF, N₂, reflux; (ii) BF₃·Et₂O, DCM; (c) i) KMnO₄, THF, H₂O; ii) H⁺; (d) CH₃OH, H₂SO₄, reflux.

Scheme 2. Synthetic routes for **P2B**, **P16B**, **PO2B** and **PO16B**.

Photophysical Properties in Solutions

The UV-vis absorption and fluorescence emission spectra of **P2B**, **P16B**, **PO2B** and **PO16B** in different solvents were shown in Figure 1 and S1, and the corresponding photophysical data were summarized in Table S1. It was clear that **P2B** exhibited three obvious absorption bands located at ca. 280 nm, ca. 310 nm and ca. 420 nm in non-polar and polar solvents (Figure 1a). The two weak absorption bands appeared at ca. 280 nm and ca. 310 nm were attributed to π - π^* transitions, and the maximum absorption peak at ca. 420 nm was originated from intermolecular charge transfer (ICT) transition, which could be confirmed by its solvent-dependent fluorescence emission spectra and fluorescence quantum yields, as well as DFT theoretical calculations. As shown in Figure 1c, **P2B** gave one strong emission at 501 nm with a shoulder at 530 nm in cyclohexane. From Figure S2 we could find that **P2B** emitted bright green light in cyclohexane under UV irradiation. With the increasing solvent polarity the emission of **P2B** was broadened and red-shifted significantly, for instance, **P2B** emitted bright orange light centered at 600 nm in DCM

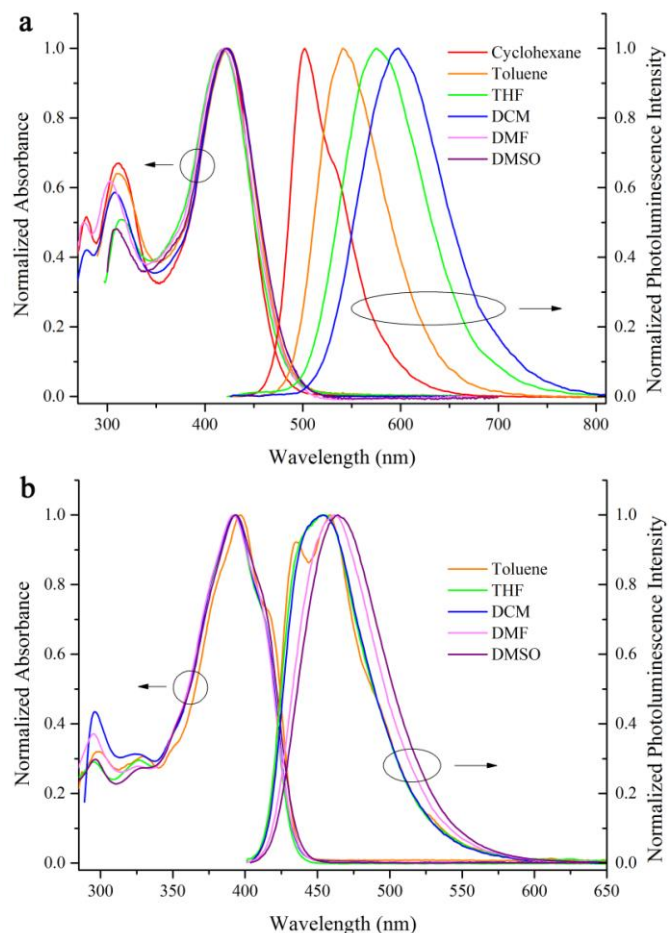


Figure 1. Normalized UV-vis absorption spectra of **P2B** (a) and normalized fluorescent emission spectra of **P2B** (b) and **PO2B** (d) excited at 420 nm and 395 nm, respectively, in different solvents (1.0×10^{-5} mol/L).

(Figure 1b and S2). We found a linear relationship between the maximum emission energy and the solvent polarity $E_T(30)$ (Figure S3). Meanwhile, the fluorescence quantum yield (Φ_F) of **P2B** decreased obviously with increasing solvent polarity. The Φ_F was 0.58 in cyclohexane and decreased to 0.03 in DMSO using 9,10-diphenylanthracene ($\Phi_F = 0.85$, in benzene) as a standard. Therefore, the linear relationship between the maximum emission energy and $E_T(30)$, and the broadening of the emission band, decreasing of Φ_F , increasing Stokes shift (3681 – 7829 cm⁻¹) with increasing solvent polarities suggested that the emission at low energy region for **P2B** was derived from ICT transition.²⁴ As shown in Figure S1a-b, compound **P16B** gave similar UV-vis absorption and fluorescence emission spectra to **P2B** because their conjugated π -skeletons were same. When phenothiazine-*S,S*-dioxide was linked to β -iminoenolate boron moiety, **PO2B** gave three absorption bands at ca. 300 nm, ca. 330 nm and ca. 395 nm in non-polar and polar solvents (Figure 1c). The two former ones were also due to π - π^* transitions, but the absorption at ca. 395 nm could be ascribed to n - π^* instead of ICT transition. The reason might be that the introduction of phenothiazine with strong electron-donating ability into β -iminoenolate boron afforded D- π -A

conjugated system with moderated polarity, leading to the occurrence of ICT. However, phenothiazine-*S,S*-dioxide was not a good electronic donor, so the polarity of **PO2B** was weak and no ICT emission could be detected. From Figure S2, we could find that **PO2B** emitted strong blue light in non-polar and polar solvents. As shown in Figure 1d, **PO2B** gave two emission bands at 436 nm and 459 nm in toluene, exhibiting vibration structures. In polar solvents of THF, DCM, DMF and DMSO the maximum emission bands of **PO2B** were located at 454 nm, 455 nm, 461 nm and 464 nm, respectively. It meant that the emission band did not shift obviously with increasing solvent polarity. Notably, the Φ_F of **PO2B** increased with the increasing solvent polarity, for example, it was 0.24 in toluene and reached to 0.70 in DMSO. Such negative solvatokinetic effect for Φ_F was also observed in β -iminoenolate boron complexes in our previous work.^{11b} Accordingly, **PO16B** showed similar absorption and fluorescent emission properties to **PO2B** in solutions (Figure S1c-d). The high quantum yields of **PO2B** and **PO16B** made them be potential fluorescent sensors in more polar solvents.

Electrochemical Properties

Cyclic voltammograms of **P2B** and **PO2B** were shown in Figure S4. **P2B** exhibited two reversible reduction processes and the halfwave potentials were located at -2.31 V and -2.47 V (*vs* Fc/Fc⁺), respectively. **PO2B** exhibited one reduction process with halfwave potential of -1.56 V (*vs* Fc/Fc⁺). The lower reductive half-wave potential of **P2B** than **PO2B** suggested stronger electron donating ability of phenothiazine than phenothiazine-*S,S*-dioxide. Additionally, the LUMO energy level was estimated according to the equation of $E_{\text{LUMO}} = -(E_{\text{red}} + 4.8)$, and the HOMO energy level was calculated using the empirical equation of $E_{\text{HOMO}} = E_{\text{LUMO}} - E_g$, in which E_g was estimated from the onset of the absorption spectrum ($E_g = 1240/\lambda_{\text{onset}}$) since we could not gain the oxidation potential under our experimental condition. In the cases of **P2B** and **PO2B**, their HOMO energy levels were located at -5.06 eV and -6.10 eV, and their LUMO energy levels were located at -2.49 eV and -3.24 eV, respectively (Table 1).

Table 1. Electrochemical data and HOMO/LUMO energy levels of **P2B** and **PO2B**.

	E_{red} (V) ^a	LUMO (eV) ^b	HOMO (eV) ^b	E_g (eV) ^c	LUMO (eV) ^d	HOMO (eV) ^d
P2B	-2.31, -2.47	-2.49	-5.06	2.57	-1.83	-4.71
PO2B	-1.56	-3.24	-6.10	2.86	-1.99	-5.65

^a E_{red} = reduction potential; Fc/Fc⁺ was used as external reference.

^b Calculated using the empirical equation: $E_{\text{LUMO}} = -(E_{\text{red}} + 4.8)$ and $E_{\text{HOMO}} = E_{\text{LUMO}} - E_g$.

^c Estimated from the onset of the absorption spectra ($E_g = 1240 / \lambda_{\text{onset}}$).

^d Obtained from quantum chemical calculation using TDDFT/B3LYP/6-31G(d)

Density Functional Theoretical Calculation

The density functional theory (DFT) calculations by Gaussian 09W program^{25a} using DFT/B3LYP/6-31G(d) method was

carried out to reveal the difference of the electronic structures for **P2B** and **PO2B**. The frontier orbital plots of the HOMO and LUMO were shown in Figure 2. It was found that the HOMO and LUMO of **P2B** were mainly distributed in electron donor (phenothiazine unit) and electron acceptor (β -iminoenolate boron moiety), respectively. Meanwhile, the absorption wavelengths (λ_{abs}), excitation energies (E_x), oscillator strengths (f) and dominant excitation characters of **P2** were calculated with TD-DFT/B3LYP/6-31G(d) method and summarized in Table S3. According to the results, the maximum absorption peak was derived from HOMO→LUMO transition. Because the frontier orbital plots of HOMO and LUMO for **P2** were mainly located at the donor and acceptor units, respectively, the maximum absorption was ascribed to ICT transition.^{25b} In the case of **PO2B**, the HOMO was distributed in the whole molecule and the LUMO was distributed in the acceptor. We deemed that the weaker polarity of **PO2B** led to the absence of ICT transition. Meanwhile, we found that the calculated HOMO and LUMO energy levels of **PO2B** were also lower than **P2B** (Table 1), similar to those obtained from electrochemical data, further illustrating the strong electron-donating ability of phenothiazine in **P2B**.^{10b}

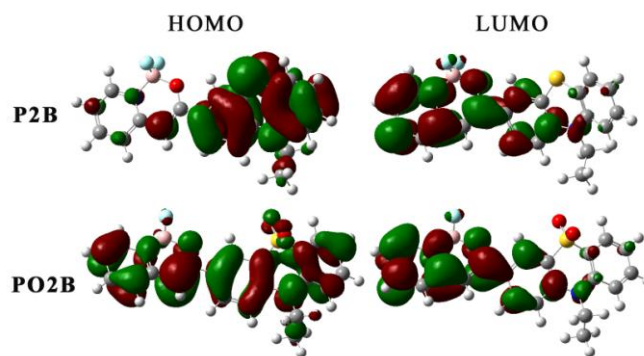


Figure 2. The frontier orbital plots of the HOMO and LUMO of **P2B** and **PO2B**.

Mechanofluorochromic Properties

We have previously found that some phenothiazine-based conjugated compounds exhibited MFC properties and the non-planar architecture of phenothiazine as well as ICT feature of D- π -A system were favorable for mechanofluorochromism.¹⁰ Herein, we intended to study the electronic effects of phenothiazine and phenothiazine-*S,S*-dioxide on the MFC properties of β -iminoenolate boron complexes since the conformations of phenothiazine and phenothiazine-*S,S*-dioxide were same. As shown in Figure 3, the β -iminoenolate boron complexes bearing phenothiazine (**P2B** and **P16B**) with ICT emission exhibited high-contrast MFC behaviors. Slight difference of the emitting colors was detected in the as-synthesized crystals and ground powders of **PO2B** without ICT emission. In addition, we found that the emitting color for **PO16B** did not change after grinding the as-synthesized crystals. To further reveal the MFC properties of **P2B** the fluorescence emission spectra in different solid states were

shown in Figure 4a. It was clear that the as-synthesized crystals of **P2B** gave two emission bands at 531 nm and 680 nm, and the emitting color was brown. When the as-synthesized crystals were ground, **P2B** emitted deep orange-red light centered at 605 nm. Interestingly, the ground powders of **P2B** showed different response to organic solvent fuming and thermal heating. When the ground powders of **P2B** were fumed with DCM for 5 s, the emission band blue-shifted to 548 nm with a big tailor in the range of 670-750 nm, and it changed into the samples emitting bright yellow light. However, the solids with

compounds. Therefore, the powder wide angle XRD patterns of **P2B** in different solid states were shown in Figure 4b. It was clear that the as-synthesized samples of **P2B** gave several sharp and strong diffraction peaks, suggesting well-ordered crystalline state. After the as-synthesized crystals of **P2B** were ground, the diffraction peaks became very weak, indicating the crystalline state was damaged into amorphous state. When the ground powders were fumed with DCM or heated, strong diffraction peaks appeared again, meaning the molecules in amorphous state could be rearranged into ordered crystalline

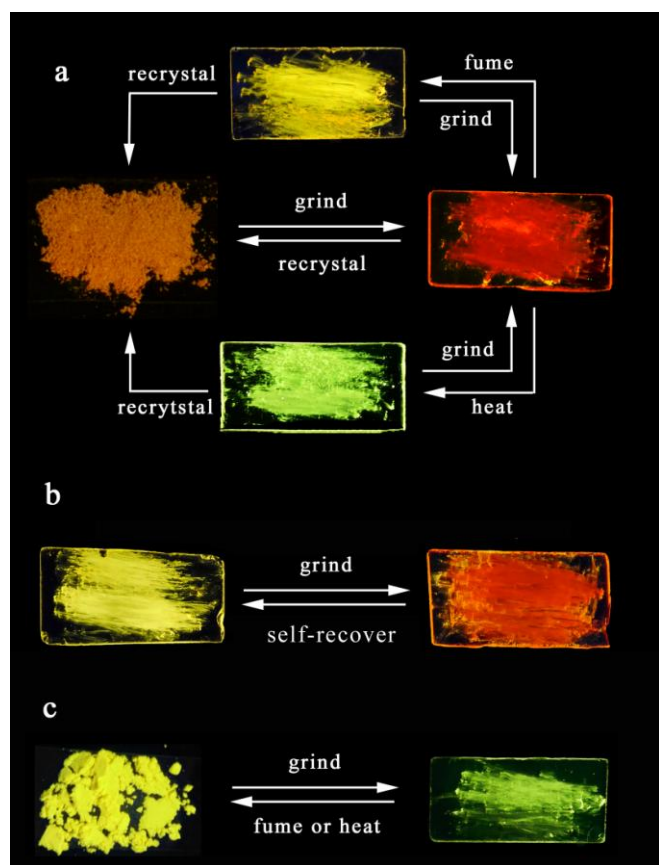


Figure 3. Photos of **P2B** (a), **P16B** (b) and **PO2B** (c) in different solid states under UV light (365 nm).

yellowish green emission centered at 526 nm could be generated after the ground powders of **P2B** were heated at 160 °C for 3 s. When the fumed and heated samples were reground, the emitting color changed to deep orange-red again. The ground powders could also be converted back to emit yellowish green light or bright yellow light upon heated or fumed with DCM (Figure S5). As a result, the emitting color of **P2B** could be transferred between deep orange-red and yellowish green reversibly through grinding and heating treatment, and could be transferred between deep orange-red and bright yellow reversibly via grinding and DCM fuming treatment. It should be noted that the brown powders could be gained via recrystallization of ground, fumed or heated samples. It is known that the molecular packing modes in different solid states would lead to different emission of organic conjugated

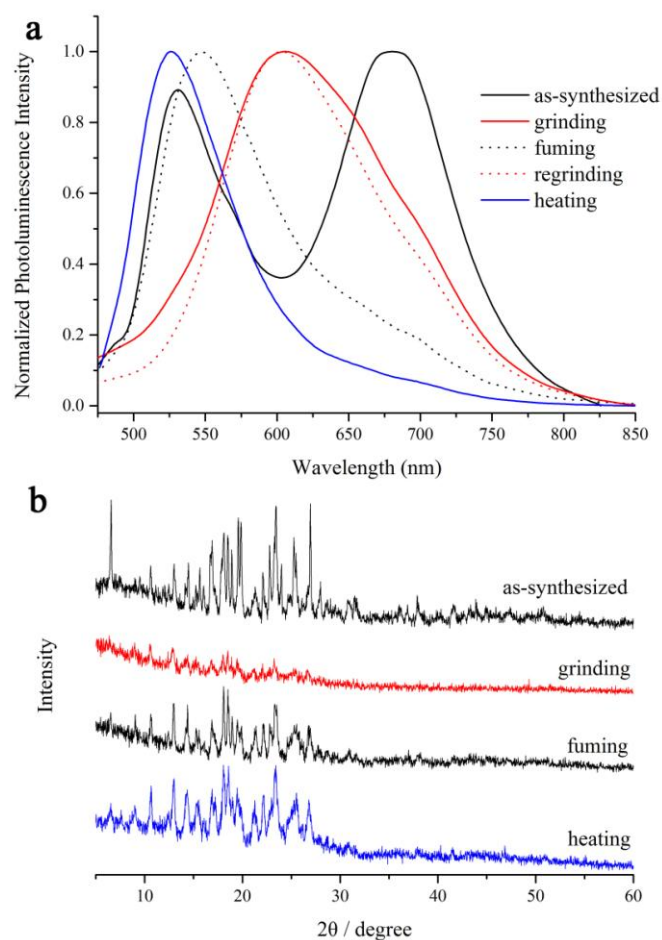


Figure 4. Fluorescent emission spectra (a, $\lambda_{\text{ex}} = 440 \text{ nm}$) and XRD patterns (b) of **P2B** in different solid states.

state. However, the diffraction peak appeared at 2θ of 6.58° (corresponding to a d -spacing of 13.4 \AA) in the as-synthesized crystals of **P2B** could not be recovered in the fumed/heated samples (Figure S6). It indicated that the long-range ordering in fumed/heated samples was poorer than that in the as-synthesized crystals. DSC curves of **P2B** could further confirm the different molecular arrangement in different solid states. The as-synthesized crystals gave only one strong endothermic peak at $199.0 \text{ }^\circ\text{C}$, corresponding to its melting point, while other two weak exothermic transition peaks at $61.0 \text{ }^\circ\text{C}$ and $82.0 \text{ }^\circ\text{C}$ appeared in the ground powders of **P2B**, which could be ascribed to the transformation from amorphous to crystalline

state (Figure 5). As a result, we deduced that the emitting color changes were due to the transformation between the crystalline and amorphous states. To well understand the mechanism of such MFC phenomenon, the UV-vis spectra measured in a reflection way and fluorescent lifetimes (τ) of **P2B** in different solid states were obtained. It was found that the as-synthesized crystals of **P2B** showed two strong broad absorption bands at ca. 450 nm and 570 nm (Figure S7). However, from Figure 1a the maximum absorption of **P2B** in dilute cyclohexane was located

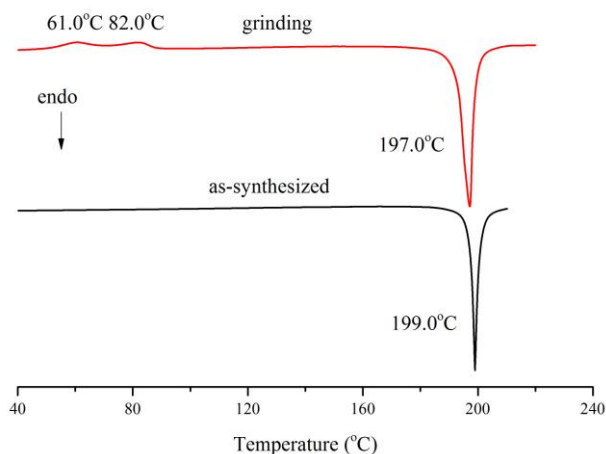


Figure 5. DSC curves of **P2B** in as-synthesized crystals (black) and ground powders (red).

at 423 nm, and no absorption appeared over 500 nm. Therefore, we suggested that the absorption at 570 nm in the as-synthesized crystals was due to the electronic transitions from the π -aggregates. Although the absorption band at ca. 450 nm for **P2B** in as-synthesized crystals showed a red-shift compared with that in cyclohexane, we deemed that it mainly came from the electronic transitions from the isolated molecules. The lifetime of the emission at 501 nm from the monomers of **P2B** in dilute cyclohexane was 4.58 ns (Table S2). In the case of the as-synthesized crystals of **P2B**, the τ values for the emission at ca. 531 nm and 680 nm were 2.52 ns and 3.85 ns, respectively, which were shorter than that in solution. Therefore, we deduced that no excimers were formed in the as-synthesized crystals, and the emission at ca. 680 nm was derived from the π -aggregates. When the as-synthesized **P2B** was ground, the crystalline structure was damaged so that the absorption band at ca. 570 nm disappeared (Figure S7) and the emission band at 680 nm decreased significantly (Figure 4). Meanwhile, **P2B** in ground powders gave an absorption band at ca. 490 nm and a broad emission band centered at 605 nm, which were red-shifted compared with those of isolated molecules on account of intermolecular π - π interactions. It should be noted that the long-range ordered π -aggregates in as-synthesized crystals could be destroyed by grinding, but π - π interactions still occurred in amorphous states since the fluorescence lifetime was prolonged in amorphous state (4.58 ns) compared with that in crystalline state (3.85 ns). After fumed, the molecules rearranged into ordered state, but we only found one emission

band at ca. 548 nm and one absorption band at ca. 450 nm from monomers, which was quite different from those in the as-synthesized crystals. The absence of the emission at ca. 680 nm and the absorption at ca. 570 nm in fumed samples was because the destroyed π -aggregates by grinding could not be reformed, which was in accordance with the irrevocable diffraction peak at 2θ of 6.58° (Figure 4b). In other words, although the amorphous state could be recovered into crystalline state upon fuming the ground powders of **P2B**, the long-range ordered π -aggregates could be not reformed again. On the other hand, the absorption band of **P2B** also blue-shifted to ca. 450 nm upon heating the ground powders due to molecular rearrangement. However, the emission of the heated samples blue-shifted to 526 nm. The different emitting colors for the fumed and heated samples might be due to the slight difference in molecular stacking.

Although the conjugated skeletons of **P16B** and **P2B** were same, **P16B** with long carbon chain showed different MFC

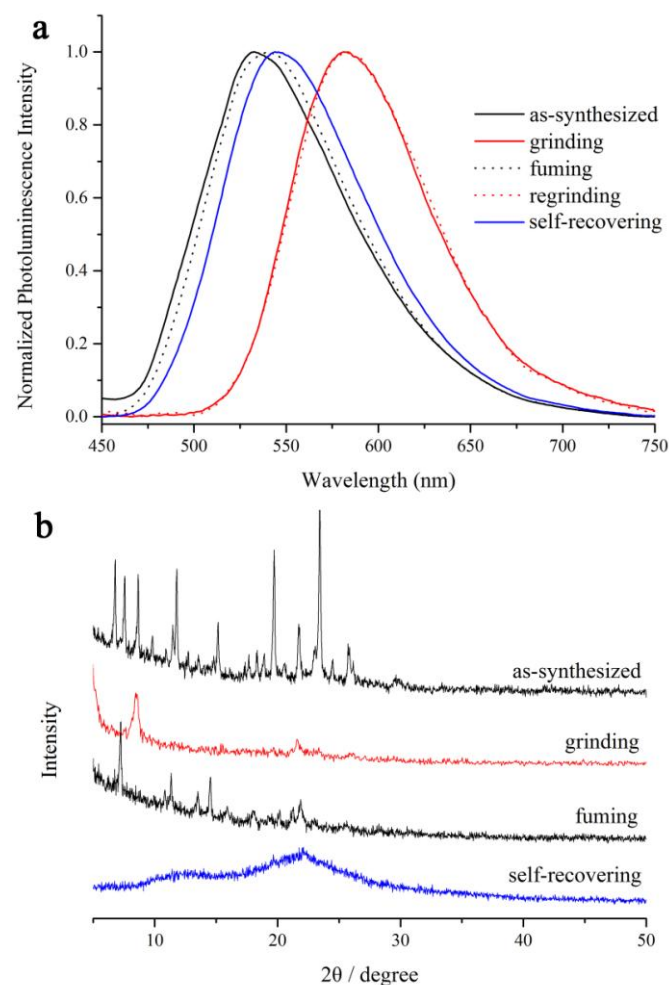


Figure 6. Fluorescent emission spectra (a, $\lambda_{ex} = 400$ nm) and XRD patterns (b) of **P16B** in different solid states.

behaviors from **P2B**. The as-synthesized crystals of **P16B** emitted bright yellow light centered at 534 nm (Figure 3 and

6a), and changed into ground powders with orange emission (582 nm) upon grinding. Moreover, the emitting color could be recovered to yellow (ca. 540 nm) after the ground powders of **P16B** were fumed with DCM for 5 s or put at room temperature for 5 min. The color transformation for the solids of **P16B** was well reversible by the treatment of grinding/fuming or self-recovering (Figure S8). Unlike **P2B**, which exhibited different emission in the as-synthesized, ground, fumed and heated states, only two different emitting colors were detected for **P16B** in different solid states. XRD patterns were measured to understand the emitting color changes between different solid states of **P16B**. As shown in Figure 6b and S9, the as-synthesized samples gave sharp and strong diffraction peaks, indicating its well-organized crystalline structure. Most of the diffraction peaks disappeared for the ground powders, so the crystalline structure was destroyed to yield amorphous state after grinding the as-synthesized crystals of **P16B**. When the ground powders were fumed with DCM, several sharp diffraction peaks emerged, suggesting the recovery of the crystalline structure. However, when the ground powders were put at room temperature for 5 min, broad diffraction peaks were observed. We deemed that the organized molecular stacking existed in the self-recovered sample, but the orderliness was not as good as that in the fumed sample. The DSC curves of **P16B** in different states were shown in Figure S10, and only one endothermic peak at 74.0 °C corresponding to the melting point appeared in the as-synthesized crystals and in the ground powders. The absence of the endothermic peak corresponding to the transformation from amorphous to crystalline state was due to the easy transformation from amorphous to crystalline states even at room temperature. Additionally, the endothermic peak appeared at ca. -5 °C for the ground powders of **P16B** was glass transition temperature. The self-recovery to crystalline from amorphous state for **P16B** at room temperature suggested that the introduction of long alky chain in MFC dye improved the reversibility of MFC.^{11c} In other words, the long carbon chain could decrease the stability of the amorphous state. Additionally, UV-vis spectra and fluorescent lifetimes of **P16B** in different solid states were also shown in Supporting Information. Similar to **P2B**, the absorption at ca. 450 nm and the emission at 534 nm for **P16B** in the as-synthesized crystals were mainly ascribed to the electronic transition from the isolated molecules (Figure S11 and 6). The short fluorescent lifetime (2.52 ns) of the emission for **P16B** in the crystals compared with that in cyclohexane (4.70 ns) illustrated that no excimers were formed. When the as-synthesized crystals were ground, the crystalline structure was damaged, and the emission of **P16B** red-shifted to 582 nm. We deduced that π - π interactions in the ground powders led to the red-shift of the emission and the prolonging of the fluorescence lifetime (4.71 ns) since the intermolecular distances would be decreased under grinding. When the ground powders were fumed with DCM, the crystalline structure recovered and the emission at 540 nm ($\tau = 2.99$ ns) from the monomers appeared again. The reason why **P16B** and **P2B** gave different MFC properties might be that the long alky chain in **P16B** would limit the π - π

interactions and restrain the formation of the long-range ordered π -aggregates.²⁶

Furthermore, we found that phenothiazine-*S,S*-dioxide functionalized β -iminoenolate boron complex **PO2B** showed low-contrast MFC behaviors compared with **P2B**. As shown in Figure 7a, **PO2B** emitted yellow light centered at 545 nm in as-synthesized crystals, which blue-shifted to 518 nm (emitting yellowish green light) in the ground powders. The emitting color could be recovered to yellow when the ground powders were fumed with DCM for 5 s or heated at 160 °C for 3 s. The MFC behaviors were reversible under the treatment of grinding/fuming or heating (Figure S12). The XRD patterns of **PO2B** in different solid states also illustrated that the transformation between amorphous and crystalline states led to the reversible MFC properties (Figure 7b and S13). Additionally, the ground powders of **PO2B** gave two exothermic peaks at 114.0 °C and 129.0 °C except for the peak corresponding to melting point (Figure S14), which further indicated the transformation from amorphous to crystalline state. Besides the melting temperature (278.0 °C), the glass transition temperature (135.0 °C) was also observed in as-

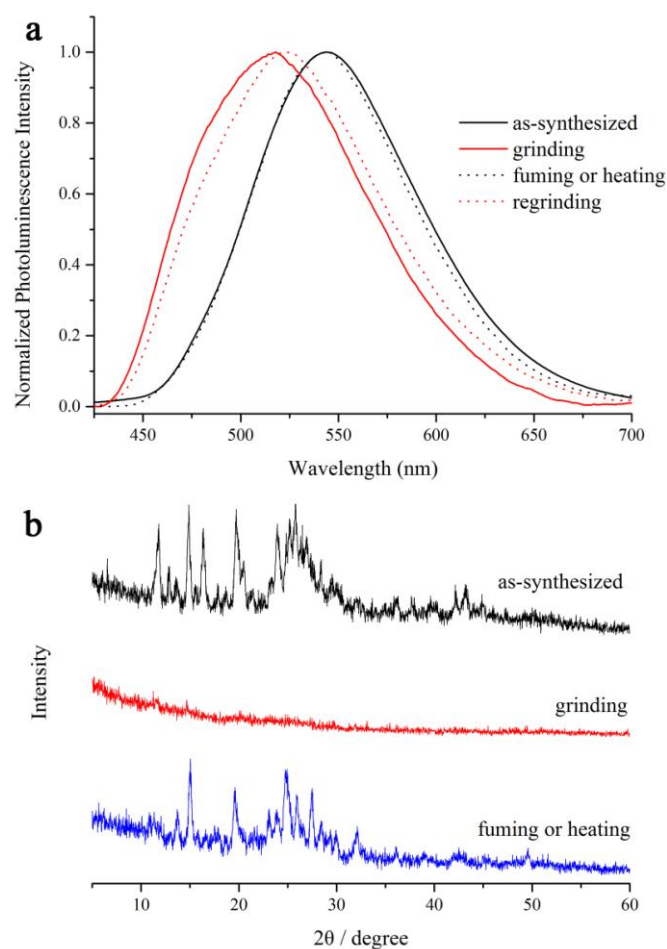


Figure 7. Fluorescent emission spectra (a, $\lambda_{\text{ex}} = 365$ nm) and XRD patterns (b) of **PO2B** in different solid states.

synthesized crystals. Meanwhile, **PO2B** showed the absorbance located at 430 nm in the as-synthesized crystals, giving a red-shift of 33 nm compared with that in dilute toluene. Notably, the τ of the emission at 545 nm in the as-synthesized crystals was 6.49 ns, which was much larger than that at 460 nm in toluene (0.54 ns). We deduced that the emission in as-synthesized crystals of **PO2B** was mainly derived from the excimers. When the as-synthesized crystals were ground into amorphous state, excimers were damaged. Therefore, the emission band of **PO2B** in ground powders blue-shifted to 518 nm with τ of 4.42 ns. Due to the significant red-shift of the absorption of **PO2B**, we deduced that π - π interactions happened in ground powders. When the ground powders were fumed with DCM or heated, the crystalline structure and the emission from excimers were recovered (Table S2). However, no MFC property could be observed for **PO16B**. From the above results, we could make the conclusion that the D- π -A conjugated system with ICT emission might give high-contrast MFC property and the introduction of long carbon chain would improve the reversibility of MFC dyes.

Conclusions

In summary, we synthesized β -iminoenolate boron complexes bearing non-planar phenothiazine (**P2B** and **P16B**) and phenothiazine-*S,S*-dioxide (**PO2B** and **PO16B**). It was found that the D- π -A type **P2B** and **P16B** gave ICT emission, while no ICT emission was observed for **PO2B** and **PO16B** due to the weak electron-donating ability of phenothiazine-*S,S*-dioxide. Interestingly, **P2B** and **P16B** with ICT emission exhibited high-contrast MFC behaviors compared with that of **PO2B** without ICT emission. For example, the as-synthesized crystals of **P2B** gave two emission bands at 531 nm and 680 nm, derived from monomers and π -aggregates, respectively. After ground, the amorphous ground powders emitted deep orange-red light located at 605 nm due to the π - π interactions between the monomers. After fumed with DCM or heated at 160 °C, the crystalline structure was recovered, and they emitted bright yellow (548 nm) or yellowish green (526 nm) light, respectively. The color changes from deep orange-red to bright yellow or yellowish green were reversible via repeating grinding and fuming or heating. On account of the formation of π -aggregates in as-synthesized crystals of **P2B**, several channels for the changes of emitting colors were provided. Although the π -conjugated skeleton of **P16B** was same as that of **P2B**, the introduction of long carbon chain restrained the formation of π -aggregates, leading to different MFC properties. The as-synthesized crystals of **P16B** emitting yellow light centered at 533 nm could be changed into ground powders emitting orange light located at 582 nm upon grinding. It should be noted that the amorphous state of **P16B** could be self-recovered to crystalline state when put at room temperature for 5 min. We deemed that the reason why **P16B** showed better reversible MFC behaviors was that the long carbon chain would decrease the stability of amorphous state via limiting the π - π interactions. In the case of **PO2B** without ICT emission, low-

contrast MFC properties were observed. The as-synthesized crystals emitted yellow light centered at 545 nm from the excimers. After grinding, the amorphous state emitted yellowish green light centered at 518 nm. Similarly, the MFC processes were also reversible under the treatment of grinding/fuming or heating. Additionally, no MFC property was detected for **PO16B**, in which long carbon chain was involved, without ICT emission. Therefore, it suggested that the introduction of non-planar conjugated unit and the construction of D- π -A system with ICT emission were favorable for the design of MFC dyes with high-contrast changes in emitting colors. In addition, the introduction of long carbon chain could improve the MFC reversibility so as to gain self-recovering MFC materials. This work is helpful for the design of novel MFC dyes.

Acknowledgements

This work is financially supported by the National Natural Science Foundation of China (21374041), the Open Project of State Key Laboratory of Supramolecular Structure and Materials (SKLSSM2015014).

Notes and references

^a State Key Laboratory of Supramolecular Structure and Materials, College of Chemistry, Jilin University, Changchun, P. R. China. E-mail: luran@mail.jlu.edu.cn

[†] Electronic Supplementary Information (ESI) available: ¹H NMR, ¹³C NMR, MALDI-TOF MS spectra; photophysical data; UV-vis absorption spectra. See DOI: 10.1039/b000000x/

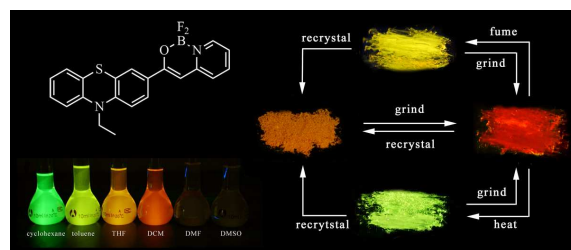
- 1 a) Z. G. Chi, X. Q. Zhang, B. J. Xu, X. Zhou, C. P. Ma, Y. Zhang, S. W. Liu and J. R. Xu, *Chem. Soc. Rev.*, 2012, **41**, 3878-3896; b) X. Q. Zhang, Z. G. Chi, Y. Zhang, S. W. Liu and J. R. Xu, *J. Mater. Chem. C*, 2013, **1**, 3376-3390.
- 2 a) M. S. Kwon, J. Gierschner, J. Seo and S. Y. Park, *J. Mater. Chem. C*, 2014, **2**, 2552-2557; b) X. Cheng, D. Li, Z. Y. Zhang, H. Y. Zhang and Y. Wang, *Org. Lett.*, 2014, **16**, 880-883; c) Y. J. Zhang, J. W. Sun, G. L. Zhuang, M. Ouyang, Z. W. Yu, F. Cao, G. X. Pan, P. S. Tang, C. Zhang and Y. G. Ma, *J. Mater. Chem. C*, 2014, **2**, 195-200.
- 3 a) A. Pucci, F. D. Cuia, F. Signori and G. Ruggeri, *J. Mater. Chem.*, 2007, **17**, 783-790; b) M. Kinami, B. R. Crenshaw and C. Weder, *Chem. Mater.*, 2006, **18**, 946-955.
- 4 a) W. Z. Yuan, Y. G. Gong, S. M. Chen, X. Y. Shen, J. W. Y. Lam, P. Lu, Y. W. Lu, Z. M. Wang, R. R. Hu, N. Xie, H. S. Kwok, Y. M. Zhang, J. Z. Sun and B. Z. Tang, *Chem. Mater.*, 2012, **24**, 1518-1528; b) Y. Y. Gong, Y. R. Zhang, W. Z. Yuan, J. Z. Sun, and Y. M. Zhang, *J. Phys. Chem. C*, 2014, **118**, 10998-11005; c) Y. Y. Gong, Y. Q. Tan, J. Liu, P. Lu, C. F. Feng, W. Z. Yuan, Y. W. Lu, J. Z. Sun, G. F. He and Y. M. Zhang, *Chem. Commun.*, 2013, **49**, 4009-4011.
- 5 Y. J. Dong, B. Xu, J. B. Zhang, X. Tan, L. J. Wang, J. L. Chen, H. G. Lv, S. P. Wen, B. Li, L. Ye, B. Zou, and W. J. Tian, *Angew. Chem. Int. Ed.*, 2012, **51**, 10782-10785.
- 6 a) W. Z. Yuan, Y. Q. Tan, Y. Y. Gong, P. Lu, J. W. Y. Lam, X. Y. Shen, C. F. Feng, H. H-Y. Sung, Y. W. Lu, I. D. Williams, J. Z. Sun,

- Y. M. Zhang and B. Z. Tang, *Adv. Mater.*, 2013, **25**, 2837-2843; b) H. Li, Z. Chi, B. Xu, X. Zhang, X. Li, S. Liu, Y. Zhang and J. Xu, *J. Mater. Chem.*, 2011, **21**, 3760-3767; c) Q. K. Qi, J. B. Zhang, B. Xu, B. Li, S. X. A. Zhang and W. J. Tian, *J. Phys. Chem. C*, 2013, **117**, 24997-25003; d) M. P. Aldred, G. F. Zhang, C. Li, G. Chen, T. Chen and M. Q. Zhu, *J. Mater. Chem. C*, 2013, **1**, 6709-6718; e) C. P. Ma, B. J. Xu, G. Y. Xie, J. J. He, X. Zhou, B. Y. Peng, L. Jiang, B. Xu, W. J. Tian, Z. G. Chi, S. W. Liu, Y. Zhang and J. R. Xu, *Chem. Commun.*, 2014, **50**, 7374-7377.
- 7 a) X. Zhang, Z. Chi, J. Zhang, H. Li, B. Xu, X. Li, S. Liu, Y. Zhang and J. Xu, *J. Phys. Chem. B*, 2011, **115**, 7606-7611; b) H. Li, X. Zhang, Z. Chi, B. Xu, W. Zhou, S. Liu, Y. Zhang and J. Xu, *Org. Lett.*, 2011, **13**, 556-559; c) Y. J. Dong, J. B. Zhang, X. Tan, L. J. Wang, J. L. Chen, B. Li, L. Ye, B. Xu, B. Zou and W. J. Tian, *J. Mater. Chem. C*, 2013, **1**, 7554-7559.
- 8 a) J. Kunzleman, M. Kinami, B. R. Crenshaw, J. D. Protasiewicz and C. Weder, *Adv Mater.*, 2008, **20**, 119-122; b) S. J. Yoon, J. W. Chung, J. Gierschner, K. S. Kim, M. G. Choi, D. Kim and S. Y. Park, *J. Am. Chem. Soc.*, 2010, **132**, 13675-13683; c) S. J. Yoon and S. Y. Park, *J. Mater. Chem.*, 2011, **21**, 8338-8346; d) J. W. Sun, X. J. Lv, P. J. Wang, Y. J. Zhang, Y. Y. Dai, Q. C. Wu, M. Ouyang and C. Zhang, *J. Mater. Chem. C*, 2014, **2**, 5365-5371.
- 9 a) G. Zhang, J. Lu, M. Sabat and C. L. Fraser, *J. Am. Chem. Soc.*, 2010, **132**, 2160-2162; b) G. Zhang, J. P. Singer, S. E. Kooi, R. E. Evans, E. L. Thomas and C. L. Fraser, *J. Mater. Chem.*, 2011, **21**, 8295-8299; c) N. D. Nguyen, G. Zhang, J. Lu, A. E. Sherman and C. L. Fraser, *J. Mater. Chem.*, 2011, **21**, 8409-8415; d) G. Zhang, J. Lu and C. L. Fraser, *Inorg. Chem.*, 2010, **49**, 10747-10749; e) T. Liu, A. D. Chien, J. Lu, G. Zhang and C. L. Fraser, *J. Mater. Chem.*, 2011, **21**, 8401-8408; f) P. Galer, R. C. Korošec, M. Vidmar and B. Šket, *J. Am. Chem. Soc.*, 2014, **136**, 7383-7394.
- 10 a) P. C. Xue, P. Chen, J. H. Jia, Q. X. Xu, J. B. Sun, B. Q. Yao, Z. Q. Zhang and R. Lu, *Chem. Commun.*, 2014, **50**, 2569-2571; b) P. C. Xue, B. Q. Yao, P. P. Wang, J. B. Sun, Z. Q. Zhang and R. Lu, *RSC Adv.*, 2014, **4**, 58732-58739; c) X. Zhang, J. Wang, J. Ni, L. Zhang and Z. Chen, *Inorg. Chem.*, 2012, **51**, 5569-5579.
- 11 a) P. C. Xue, B. Q. Yao, J. B. Sun, Q. X. Xu, P. Chen, Z. Q. Zhang and R. Lu, *J. Mater. Chem. C*, 2014, **2**, 3942-3950; b) Z. Q. Zhang, P. C. Xue, P. Gong, G. H. Zhang, J. Peng and R. Lu, *J. Mater. Chem. C*, 2014, **2**, 9543-9551; c) P. C. Xue, B. Q. Yao, X. Liu, J. B. Sun, P. Gong, Z. Q. Zhang, C. Qian, Y. Zhang and R. Lu, *J. Mater. Chem. C*, 2015, **3**, 1018-1025; d) G. H. Zhang, J. B. Sun, P. C. Xue, Z. Q. Zhang, P. Gong, J. Peng and R. Lu, *J. Mater. Chem. C*, 2015. DOI: 10.1039/c4tc02925a.
- 12 a) J. H. Jia, K. Y. Cao, P. C. Xue, Y. Zhang, H. P. Zhou and R. Lu, *Tetrahedron*, 2012, **68**, 3626-3632; b) W. Wu, J. Yang, J. Hua, J. Tang, L. Zhang, Y. Long and H. Tian, *J. Mater. Chem.*, 2010, **20**, 1772-1779; c) Y. Hua, S. Chang, D. Huang, X. Zhou, X. Zhu, J. Zhao, T. Chen, W.-Y. Wong and W.-K. Wong, *Chem. Mater.*, 2013, **25**, 2146-2153.
- 13 a) X. F. Zhang, X. P. Qiu, R. Lu, H. P. Zhou, P. C. Xue, X. L. Liu, *Talanta*, 2010, **82**, 1943-1949; b) G. Ajayakumar, K. Sreenath and K. R. Gopidas, *Dalton T.*, 2009, 1180-1186.
- 14 a) L. Yao, S. Zhang, R. Wang, W. Li, F. Shen, B. Yang and Y. Ma, *Angew. Chem. Int. Ed.*, 2014, **53**, 2119-2123; b) X. Yang, R. Lu, P. Xue, B. Li, D. Xu, T. Xu and Y. Zhao, *Langmuir*, 2008, **24**, 13730-13735; c) H.-J. Yen and G.-S. Liou, *J. Mater. Chem.*, 2010, **20**, 9886-9894.
- 15 X. C. Yang, R. Lu, H. P. Zhou, P. C. Xue, F. Y. Wang, P. Chen, Y. Y. Zhao, *J. Colloid Interf. Sci.*, 2009, **339**, 527-532.
- 16 a) J. Lee, J.-I. Lee, M.-J. Park, Y. K. Jung, N. S. Cho, H. J. Cho, D.-H. Hwang, S.-K. Lee, J.-H. Park, J. Hong, H. Y. Chu and H.-K. Shim, *J. Polym. Sci., Part A: Polym. Chem.*, 2007, **45**, 1236-1246; b) L. Y. Yang, C. Wang, L. Q. Li, S. Janietz, A. Wedel, Y. L. Hua and S. G. Yin, *J. Polym. Sci., Part A: Polym. Chem.*, 2007, **45**, 4291-4299; c) K. T. Kamtekar, K. Dahms, A. S. Batsanov, V. Jankus, H. L. Vaughan, A. P. Monkman and M. R. Bryce, *J. Polym. Sci., Part A: Polym. Chem.*, 2011, **49**, 1129-1137; d) J. Sun, H.-J. Jiang, J.-L. Zhang, Y. Tao and R.-F. Chen, *New J. Chem.*, 2013, **37**, 977-985; e) X. Ma, X. Mao, S. Zhang, X. Huang, Y. Cheng and C. Zhu, *Polym. Chem.*, 2013, **4**, 520-527.
- 17 a) P. Ashokkumar, H. Weischoff, W. Kraus and K. Rurack, *Angew. Chem. Int. Ed.*, 2014, **53**, 2225-2229; b) N. Sakamoto, C. Ikeda, M. Yamamura and T. Nabeshim, *Chem. Commun.*, 2012, **48**, 4818-4820; c) S. Erbas-Cakmak and E. U. Akkaya, *Org. Lett.*, 2014, **16**, 2946-2949; d) J. J. Hu, N.-K. Wong, Q. Gu, X. Bai, S. Ye and D. Yang, *Org. Lett.*, 2014, **16**, 3544-3547.
- 18 a) T. Rousseau, A. Cravino, T. Bura, G. Ulrich, R. Ziessel and J. Roncali, *Chem. Commun.*, 2009, 1673-1675; b) D. Kumaresan, R. P. Thummel, T. Bura, G. Ulrich and R. Ziessel, *Chem. Eur. J.*, 2009, **15**, 6335-6339; c) Y. Kubo, D. Eguchi, As. Matsumoto, R. Nishiyabu, H. Yakushiji, K. Shigaki and M. Kaneko, *J. Mater. Chem. A*, 2014, **2**, 5204-5211; d) A. Bessette and G. S. Hanan, *Chem. Soc. Rev.*, 2014, **43**, 3342-3405.
- 19 a) T. Sarma, P. K. Panda and J.-I. Setsune, *Chem. Commun.*, 2013, **49**, 9806-9808; b) G. Ulrich, S. Goeb, A. D. Nicola, P. Retailleau and R. Ziessel, *J. Org. Chem.*, 2011, **76**, 4489-4505; c) L. Zeng, C. Jiao, X. Huang, K.-W. Huang, W.-S. Chin and J. Wu, *Org. Lett.*, 2011, **13**, 6026-6029.
- 20 a) X. L. Liu, X. F. Zhang, R. Lu, P. C. Xue, D. F. Xu and H. P. Zhou, *J. Mater. Chem.* 2011, **21**, 8756-8765; b) X. F. Zhang, R. Lu, J. H. Jia, X. L. Liu, P. C. Xue, D. F. Xu and H. P. Zhou, *Chem. Commun.*, 2010, **46**, 8419-8421; c) C. Qian, K. Y. Cao, X. L. Liu, X. F. Zhang, D. F. Xu, P. C. Xue and R. Lu, *Chinese Sci. Bull.*, 2012, **57**, 4264-4271; d) C. Qian, G. H. Hong, M. Y. Liu, P. C. Xue and R. Lu, *Tetrahedron*, 2014, **70**, 3935-3942.
- 21 a) Y. Zhou, Y. Xiao, S. M. Chi, X. H. Qian, *Org. Lett.*, 2008, **10**, 633-636; b) J. Q. Feng, B. L. Liang, D. L. Wang, L. Xue, X. Y. Li, *Org. Lett.*, 2008, **10**, 4437-4440; c) Y. Kubota, Y. Ozaki, K. Funabiki, M. Matsui, *J. Org. Chem.*, 2013, **78**, 7058-7067; d) Y. Kubota, H. Hara, S. Tanaka, K. Funabiki, Masaki Matsui, *Org. Lett.*, 2011, **13**, 6544-6547.
- 22 a) J. Kunzleman, M. Kinami, B. R. Crenshaw, J. D. Protasiewicz and C. Weder, *Adv. Mater.*, 2008, **20**, 119-122; b) M. Zheng, M. Sun, Y. Li, J. Wang, L. Bu, S. Xue, W. Yang, *Dyes Pigments*, 2014, **102**, 29-34; c) X. Zhang, Z. Ma, Y. Yang, X. Zhang, Z. Chi, S. Liu, J. Xu, X. Jia, Y. Wei, *Tetrahedron*, 2014, **70**, 924-929; d) Y. Wang, W. Liu, L. Bu, J. Li, M. Zheng, D. Zhang, M. Sun, Y. Tao, S. Xue and W. Yang, *J. Mater. Chem. C*, 2013, **1**, 856-862.
- 23 L. Kong, J.-X. Yang, Z.-M. Xue, H.-P. Zhou, L.-J. Cheng, Q. Zhang, J.-Y. Wu, B.-K. Jin, S.-Y. Zhang and Y.-P. Tian, *J. Mater. Chem. C*, 2013, **1**, 5047-5057.

- 24 J. S. Yang, K. L. Liao, C. M. Wang and C. Y. Hwang, *J. Am. Chem. Soc.*, 2004, **126**, 12325-12335.
- 25 a) M. J. Frisch, G. W. Trucks, H. B. Schlegel, G. E. Scuseria, M. A. Robb, J. R. Cheeseman, G. Scalmani, V. Barone, B. Mennucci, G. A. Petersson, H. Nakatsuji, M. Caricato, X. Li, H. P. Hratchian, A. F. Izmaylov, J. Bloino, G. Zheng, J. L. Sonnenberg, M. Hada, M. Ehara, K. Toyota, R. Fukuda, J. Hasegawa, M. Ishida, T. Nakajima, Y. Honda, O. Kitao, H. Nakai, T. Vreven, J. A. Montgomery, Jr, J. E. Peralta, F. Ogliaro, M. Bearpark, J. J. Heyd, E. Brothers, K. N. Kudin, V. N. Staroverov, R. Kobayashi, J. Normand, K. Raghavachari, A. Rendell, J. C. Burant, S. S. Iyengar, J. Tomasi, M. Cossi, N. Rega, J. M. Millam, M. Klene, J. E. Knox, J.B. Cross, V. Bakken, C. Adamo, J. Jaramillo, R. Gomperts, R. E. Stratmann, O. Yazyev, A. J. Austin, R. Cammi, C. Pomelli, J. W. Ochterski, R. L. Martin, K. Morokuma, V. G. Zakrzewski, G. A. Voth, P. Salvador, J. J. Dannenberg, S. Dapprich, A. D. Daniels, Ö. Farkas, J. B. Foresman, J. V. Ortiz, J. Cioslowski and D. J. Fox, *Gaussian 09, Revision A.02*, Gaussian, Inc., Wallingford, CT, 2009; b) M. Sun, T. Pullerits, P. Kjellberg, W. J. D. Beenken and K. Han; *J. Phys. Chem. A*, 2006, **110**, 6324-6328.
- 26 a) M. R. Molla, D. Gehrig, L. Roy, V. Kamm, A. Paul, F. Laquai and S. Ghosh, *Chem. Eur. J.*, 2014, **20**, 760-771; b) G. H. Hong, C. Qian, P. C. Xue, X. L. Liu, Q. Q. Wang, P. Gong and R. Lu, *Eur. J. Org. Chem.*, 2014, 6155-6162.

TOC For:

Mechanofluorochromic properties of β -iminoenolate boron complexes tuned by the electronic effects of terminal phenothiazine and phenothiazine-*S,S*-dioxide



β -Iminoenolate boron complex bearing phenothiazine exhibited high-contrast mechanofluorochromic behavior compared with that containing phenothiazine-*S,S*-dioxide unit.